Annals of Glaciology 38 2004

Slab avalanche release viewed as interface fracture in a random medium

Michael ZAISER
Centre for Materials Science and Engineering, The University of Edinburgh, Sanderson Building, The King's Buildings, Edinburgh EH9 3JL, Scotland
E-mail: M.Zaiser@ed.ac.uk

ABSTRACT. A theoretical model is formulated to investigate the influence of random variations in strength of the weak layer on slab avalanche release. An equation for slab stability is derived which accounts for stress redistribution between strong and weak regions. The model is first used to re-derive results on shear fractures (shear bands) in a homogeneous slab. It is then applied to the case of a slab with randomly varying peak strength of the weak layer. It is demonstrated that such variation may have a dramatic knock-down effect on the failure strength of a slope. The nature of the critical flaw is studied and precursors to failure are investigated.

1. INTRODUCTION

It is commonly agreed that dry-slab avalanche release is triggered by shear failure of a thin weak layer underlying a thick cohesive slab (Schweizer, 1999). Several authors (e.g. McClung, 1979; Bader and Salm, 1990) have invoked fracture-mechanics concepts to understand the failure process. They consider the existence of an extended flaw (termed a shear band by McClung) which is, in fact, very similar to a Griffith crack in linear elastic fracture mechanics. As in fracture mechanics, the stability of the system depends on the extension and geometry of the critical flaw.

Recently, the concept of a critical crack has been criticized by several authors (e.g. Arndt and Nattermann, 2001). It has been pointed out that, unless the nucleation problem is addressed and/or the size of pre-existing cracks can be determined experimentally, one simply replaces one unknown quantity (the failure stress) by another (the size of the critical crack). Arndt and Nattermann (2001) also demonstrated that random variations in material strength may trigger athermal crack nucleation and may therefore play a crucial role in failure of bulk materials.

Large and apparently random variations in the shear strength of weak layers have been reported by Conway and Abrahamson (1988). In their study they assess the implications for slow-slope stability by evaluating the probability of finding deficit zones where the strength of the weak layer falls below the acting (gravitational) stress. A problem of this approach is that the overlying slab may effect a stress redistribution such that a deficit zone is supported and "anchored" by surrounding stronger regions, and the situation may be further complicated by the presence and interactions of multiple deficit zones. In general, slope failure should therefore be considered as a collective process which involves both multiple local failure of the weak layer and concomitant stress redistribution to adjacent regions. To deal with such collective phenomena in slab avalanche release is the main rationale of the model which we formulate in the present paper.

2. FORMULATION OF THE MODEL

2.1. Stress redistribution in a thin slab

We consider the situation shown in Figure 1: a weak layer is running along the plane $y = d'$ in a snowpack of thickness d. For simplicity we assume the elastic constants (shear modulus G, Young's modulus E) of the snow above and below the weak layer to be the same. Following the lines of Palmer and Rice (1973) and McClung (1979), we consider a quasi-one-dimensional model: we assume the system to be homogeneous in the z direction, such that the displacement across the weak layer can be written as a function $u(x)$ of the x coordinate only. The nature of the failure depends on the angle θ between the u and x directions: for $\theta = 0$ we have mode II failure (shear failure along the weak layer propagating upslope or downslope) and for $\theta = \pi/2$ mode III failure (shear failure propagating sideways across slope). The extension of the slope is assumed much larger than any other characteristic length in the system such that we may neglect boundary effects. In generalization of previous models, we allow for random spatial variations of the shear strength of the weak layer as a function of the x coordinate.

Owing to the material inhomogeneity, J-integral methods as used by Palmer and Rice (1973) for analyzing shear band propagation do not work in the present case. Instead

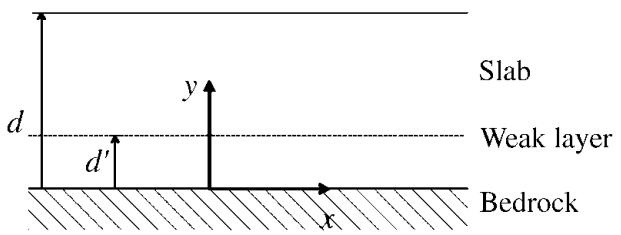

Fig. 1. Snowpack geometry considered in the model.

https://doi.org/10.3189/172756404781815040 Published online by Cambridge University Press

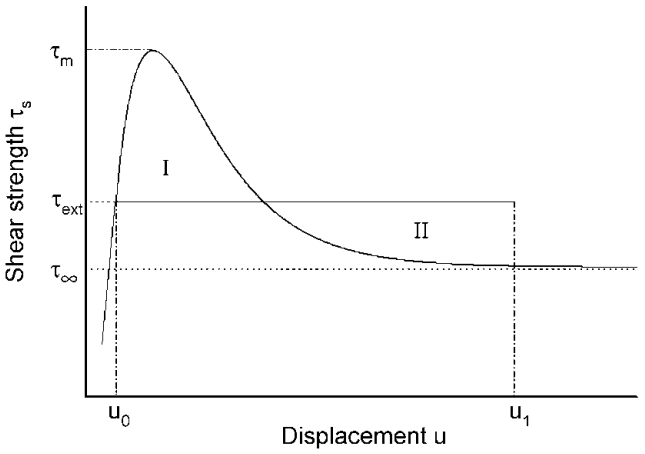

Fig. 2. Shear strength vs displacement across weak layer, and "equal-area" condition fulfilled by a shear band (schematically).

we have to explicitly consider the stress distribution which arises from a general distribution of slip $u(x)$. This can be done using a dislocation representation of the internal stresses (Weertman, 1996; Arndt and Nattermann, 2001). In particular, the internal shear stress acting at location x on the weak layer can be written as

$$\tau_{\rm int}(x) = \int \tau(x-x')\nabla_{x'}u(x')\,{\rm d}x' \,. \qquad (1)$$

Here $\tau(x)$ is the shear stress created at the point (x, d') by a dislocation of unit strength located at $(0, d')$, and $\nabla_x u(x)$ is the dislocation density associated with the inhomogeneous distribution $u(x)$ of slip in the plane $y = d'$ of the weak layer.

To evaluate the internal stresses, we have to work out the stress field of a dislocation running in the z direction on the plane $y = d'$. The dislocation is contained in a layer with elastic moduli E, G sandwiched between media with $E, G \approx \infty$ for $y < 0$ (the bedrock) and $E, G \approx 0$ for $y > d$ (the open air). The stress field depends on the dislocation character, which in turn is governed by the angle θ between the u and x directions. For $\theta = \pi/2$ (mode III failure) the crack dislocations have screw character, and we can use results given by Wang (1999) to write $\tau(x)$ as

$$\tau(x) = \frac{Gx}{2\pi}\left\{\frac{1}{x^2} + \frac{1}{x^2+4d'^2} + \sum_{n=1}^{\infty}(-1)^n\left[\frac{2}{x^2+4(nd)^2} + \frac{1}{x^2+4(nd+d')^2} + \frac{1}{x^2+4(nd-d')^2}\right]\right\}. \qquad (2)$$

We now make an important approximation: we assume that the snowpack is thin in the sense that variations in u occur on a characteristic length scale which significantly exceeds d and d'. We may then expand the slowly varying function $\nabla_{x'}u(x')$ in a Taylor series around $x' = x$: $\nabla_{x'}u(x') = \nabla_x u(x) + (x-x')\nabla_{xx}u(x) + \ldots$ Inserting into Equation (2) and retaining only the lowest-order non-vanishing term yields after some lengthy algebraic manipulations

$$\tau_{\rm int}(x) \approx I u_{xx} \,, \qquad (3)$$

where the stress redistribution factor

$$I = \int x\tau(x)\,{\rm d}x = 2(d-d')G \qquad (4)$$

turns out to be proportional to the thickness of the slab above the weak layer but does not depend on the thickness of the underlying snowpack.

For other values of θ (mode II or mixed-mode fracture) the shear stress along the weak layer can be calculated using the stress fields of edge or mixed dislocations. The final result is again of the form of Equations (3) and (4). The only difference is that I multiplies with a scalar pre-factor of the order of unity which depends on the angle θ and on the value of Poisson's ratio.

2.2. Equation for slab stability

The dependence of the shear strength of the weak layer on the shear displacement is characterized by a hardening–softening curve as shown schematically in Figure 2 (see, e.g., McClung, 1979). The shear strength increases initially towards a peak value $\tau_{\rm m}$ and then drops towards an asymptotic value τ_∞. In general, the strength–displacement curve $\tau_{\rm s}(u, x)$ may be position-dependent. In our simulations in section 4, we account for such position dependence in terms of random variations of the peak shear strength.

For the slab to be stable, the displacement field $u(x)$ must fulfil the inequality

$$I u_{xx} + \tau_{\rm ext} - \tau_{\rm s}(u, x) \le 0 \,, \qquad (5)$$

i.e. the locally acting (external and internal) stress must not exceed the local shear strength. Equation (5) is constitutive for our model. We consider rate-independent behavior, i.e. once condition (5) is violated for some x, the displacement $u(x)$ at the unstable locations increases quasi-instantaneously until a new stable configuration is reached. If no such configuration exists, u increases indefinitely and the slab fails.

3. FAILURE OF A HOMOGENEOUS SLAB BY SHEAR BAND PROPAGATION

We first consider the failure of a homogeneous slab (no strength variations) by formation and propagation of a shear band as investigated by McClung (1979). A localized shear band is characterized by a displacement field $u(x)$ which at $x \to -\infty$ starts from a value u_0 on the left stable branch of the $\tau_{\rm s}(u)$ curve, goes through a maximum u_1 which without loss of generality we assume at $x = 0$, and then reverts to u_0 for $x \to \infty$. The displacement field of a critical (marginally stable) shear band satisfies the equation

$$I u_{xx} + \tau_{\rm ext} - \tau_{\rm s}(u) = 0 \,. \qquad (6)$$

By analogy, this differential equation can be envisaged as describing the undamped motion of a particle of mass I in a potential $V = \int[\tau_{\rm ext} - \tau_{\rm s}(u)]\,{\rm d}u$. It follows that the solution must satisfy the "energy conservation" criterion $V(u_0) = V(u_1)$, and hence u_0 and u_1 must fulfil the relation

$$\int_{u_0}^{u_1} (\tau_{\rm ext} - \tau_{\rm s}(u))\,{\rm d}u = 0 \,. \qquad (7)$$

Solutions can be found for any value of the external shear stress in the range $\tau_\infty \le \tau_{\rm ext} \le \tau_{\rm m}$. A geometrical illustration is given in Figure 2: areas I and II enclosed by the line $\tau = \tau_{\rm ext}$ above and below the $\tau_{\rm s}(u)$ curve must be equal.

Approximate analytical relations can be derived if the

https://doi.org/10.3189/172756404781815040 Published online by Cambridge University Press

length of the shear band is large in comparison with that of the end region over which the strength of the weak layer drops to the residual value τ_∞. Outside the end region the displacement profile is

$$u(x) = \frac{(L-x)^2(\tau_{\rm ext}-\tau_\infty)}{2I}\,. \tag{8}$$

Hence, $u_1 = L^2(\tau_{\rm ext}-\tau_\infty)/(2I)$. The equal-area condition (7) can be written in the approximate form

$$u_1(\tau_{\rm ext}-\tau_\infty) \approx \int_{u_0}^{u_*} [\tau_{\rm ext}-\tau_{\rm s}(u)]\,{\rm d}u\,, \tag{9}$$

where u_* is the displacement where the descending branch of the stress–strain characteristics assumes the value $\tau = \tau_{\rm ext}$. Since a "long" shear band requires $\tau_{\rm ext}-\tau_\infty$ to be small, the integral on the righthand side is approximately equal to the area between the curve $\tau_{\rm s}(u)$ and the line $\tau = \tau_\infty \approx \tau_{\rm ext}$. We define the characteristic displacement $\bar u$ by

$$\int (\tau_{\rm s}(u)-\tau_\infty)\,{\rm d}u = (\tau_{\rm m}-\tau_\infty)\bar u \tag{10}$$

and, using Equations (8) and (9), we finally obtain the approximate relation

$$\frac{d-d'}{4G}\left[\frac{L(\tau_{\rm ext}-\tau_\infty)}{d-d'}\right]^2 = (\tau_{\rm m}-\tau_\infty)\bar u \tag{11}$$

for a marginally stable shear band. A band of length L is stable up to the corresponding external stress. Slope failure then occurs if either the length of the band or the external stress is increased by an infinitesimal amount. The relation (11) has been previously derived by McClung (1979) from a quite different line of reasoning. The only difference is that here we consider mode III failure, whereas McClung (1979) considers shear failure in mode II. This leads to a different combination of elastic moduli on the lefthand side of Equation (11) (McClung obtains $2E$ instead of $4G$).

Formally, the above calculations are very similar to those carried out by Zbib and Aifantis (1988) who used a second-order gradient approximation to the internal stress field to describe strain localization during shear band formation in a strain-softening material. Although we address a different problem, namely the "forward" extension of a shear band along the shear plane, the mathematical formalism is identical to that used by Zbib and Aifantis. The exercise of re-deriving relations obtained previously by other methods (see Palmer and Rice, 1973; McClung, 1979) serves us mainly to demonstrate that the "gradient" approach to internal stresses can indeed be applied to the problem at hand. We now proceed to the case which is in the focus of the present work, i.e. failure of a slope where the weak layer exhibits random variations in strength.

4. FAILURE OF A SLAB WITH RANDOM STRENGTH VARIATIONS OF THE WEAK LAYER

4.1. Simulation method

When there are random spatial variations in the strength of the weak layer, no analytical solutions are available and one has to resort to computer simulations. To obtain reliable statistics, it is desirable to simulate huge ensembles of statistically equivalent systems. To improve computational efficiency, we use a lattice automaton technique where we allow the space coordinate to take only discrete values x_i with constant spacing Δx. Accordingly, we replace u_{xx} in Equation (5) by the discrete second-order gradient. Furthermore we approximate the strength–displacement characteristics by a piecewise linear curve,

$$\tau_{\rm s}(u) = \begin{cases} \tau_\infty + (\tau_{\rm m}-\tau_\infty)[1-u/(2\bar u)], & u \le 2\bar u \\ \tau_\infty, & u > 2\bar u\,. \end{cases} \tag{12}$$

Randomness is introduced by considering the peak strength $\tau_{\rm m}$ as a random function of space. We chose Δx to be equal to the characteristic correlation length ξ of the strength variations, such that we may envisage the peak strengths at the different "sites" x_i as statistically independent random variables.

In the following, it is convenient to shift the zero of the stress axis to τ_∞ and define non-dimensional space, displacement and stress variables via

$$X = \frac{x}{\xi},\; U = \frac{u}{2\bar u},\; T = \frac{(\tau-\tau_\infty)\xi^2}{2\bar u(d-d')G}\,. \tag{13}$$

In these variables, the stability condition for the "site" X_i reads

$$\begin{aligned} &[U_{i+1}+U_{i-1}-2U_i] + T_{\rm EXT} - T_i(U_i) \le 0, \\ &T_i(U_i) = \begin{cases} T_{\rm M}^i(1-U_i), & U_i \le 1 \\ 0\,, & U_i > 1. \end{cases} \end{aligned} \tag{14}$$

The peak strengths $T_{\rm M}^i$ are assumed to be Weibull-distributed with the cumulative distribution function

$$P(T_{\rm M}) = 1 - \exp\left[-(T_{\rm M}/\bar T)^\beta\right]. \tag{15}$$

This distribution is characterized by the parameters $\bar T$ and β. In the following, we use instead the mean value $\langle T_{\rm M}\rangle$ and relative variance $\sigma_{\rm M}/\langle T_{\rm M}\rangle$ of the peak strengths, which are related to the Weibull parameters by $\langle T_{\rm M}\rangle = \bar T\Gamma(1+1/\beta)$ and $\sigma_{\rm M}/\langle T_{\rm M}\rangle = \Gamma(1+1/\beta)/[\Gamma(1+2/\beta)]^2 - 1$, where $\Gamma(x)$ denotes the gamma function. We have verified that the results remain qualitatively unchanged if other types of distribution (log-normal or box-shaped) are used.

A simulation is carried out as follows: Values of the average peak strength and peak strength variation are chosen, and random peak strengths $T_{\rm M}^i$ are assigned to all sites according to the corresponding Weibull distribution. Then the external stress $T_{\rm EXT}$ is increased from zero in small steps ΔT (this mimics slow loading as for instance by snowfall) until sites become unstable as the stress exceeds the local shear strength. The displacement at all unstable sites is increased by a small amount ΔU. Then, new internal stresses are computed for all sites and it is checked again where the sum of the external and internal stresses exceeds the local strength. The displacement at the now unstable sites is again increased, and so on. This is repeated until the system has reached a new stable configuration. Then the external stress is increased again and so on until the system has failed completely ($U_i > 1$ for all sites). The corresponding *critical stress* is denoted by $T_{\rm C}$. The procedure is repeated for different values of ΔU and ΔT to ensure that the results do not depend on step size.

Typical values and ranges of the physical parameters of our system are compiled in Table 1. From these values, we find a typical range of the non-dimensional peak shear strength $1 < T_{\rm M} < 10$. In the following we use, unless otherwise noted, the typical values $T_{\rm M} = 5$ and $\sigma_{\rm M}/\langle T_{\rm M}\rangle = 1$ for the average peak shear strength and peak strength variation.

https://doi.org/10.3189/172756404781815040 Published online by Cambridge University Press

Table 1. Typical values and ranges of the physical parameters entering the model

Parameter	*Typical value*	*Range*	*Source*
Slab depth $(d - d')$	0.5 m	0.3–1 m	Schweizer (1999)
Shear modulus G	0.5 MPa	0.1–5 MPa	Schweizer (1999)
Ratio shear modulus/peak strength (slow loading)	100	20–200	Schweizer (1999)
Ratio peak strength/residual strength	1.5	1.25–2	Schweizer (1999)
Ratio peak-strength variance/average peak strength	1	0.6–2	Conway and Abrahamson (1988)
Correlation length ξ of strength variations	1 m	0.2–1.3 m	Conway and Abrahamson (1988)
Displacement to failure u_0	4 mm	1–10 mm	McClung (1979)

4.2. Critical conditions for slope failure

Due to randomness of the local strength, the critical stress for failure of a slope of finite size is itself a random variable. The simulations indicate that the probability distribution of critical stresses is approximately Gaussian. The average failure stress decreases approximately in inverse proportion with the logarithm of system size X_S. This is plausible since large systems (large slopes) have an enhanced probability to contain very weak configurations which may fail at low stress. However, the size dependence is not strong and, in view of the fact that the range of physical system sizes is restricted ($X_S = 1000$ corresponds for $\xi = 1$ m to a slope of 1 km width), in the subsequent simulations we adopt a uniform system size of $X_S = 400$.

The average failure stress increases linearly with the average peak strength of the weak layer (insert of Fig. 3). This figure also demonstrates that the average slope failure stress falls significantly below the average peak strength of the weak layer unless the strength distribution is very narrow. This effect is pronounced even at small values of $\sigma_M/\langle T_M\rangle$: already a relative scatter of the peak strengths of the order of 20% may decrease the slope failure stress by a factor of two. This indicates the importance of localized weak configurations for triggering failure. However, as we shall see in the next section, such configurations need not necessarily conform to the idea of point-like flaws or linearly extended shear bands.

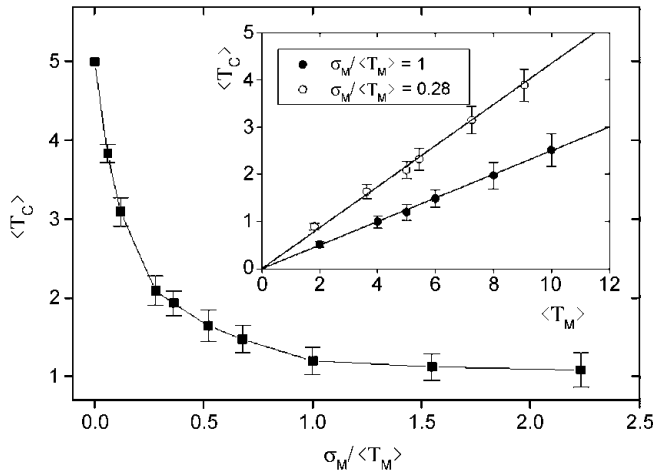

Fig. 3. Dependence of slope failure stress on the average peak strength and peak-strength variation of the weak layer. Square data points: critical stresses for average peak strength $\langle T_M\rangle = 5$ and different values of the peak-strength variation $\sigma_M/\langle T_M\rangle$. Insert: dependence of failure stress on peak strength for two different values of the relative peak-strength variation. Each data point represents an average over an ensemble of 100 systems; the error bars represent the variance of the respective failure stress distributions.

4.3. Nature of the critical flaw

To investigate the nature of the critical flaw, we define a damage function $D(x)$ which is unity at those sites where the strength of the weak layer has dropped to its residual value, and zero everywhere else. In our simulations we find that just before failure the distribution of damage is rather irregular (insert of Fig. 4). Instead of a single point-like flaw or an extended damaged area representing a shear band, one observes a "bar-code" pattern of irregular damage clusters which vaguely resembles a randomized Cantor set. To statistically characterize this pattern, we investigate the damage autocorrelation function $C(X) = \langle D(X')D(X + X')\rangle$. The average is evaluated over all values of X' and, to obtain reliable statistics, we further average over an ensemble of many systems. Up to a characteristic damage correlation length $X_C \approx 25$ we observe a power-law decay $C(X) \propto X^{-m}$, where $m \approx 0.46$. This implies that, below X_C, the damage distribution can be described as a random fractal set with

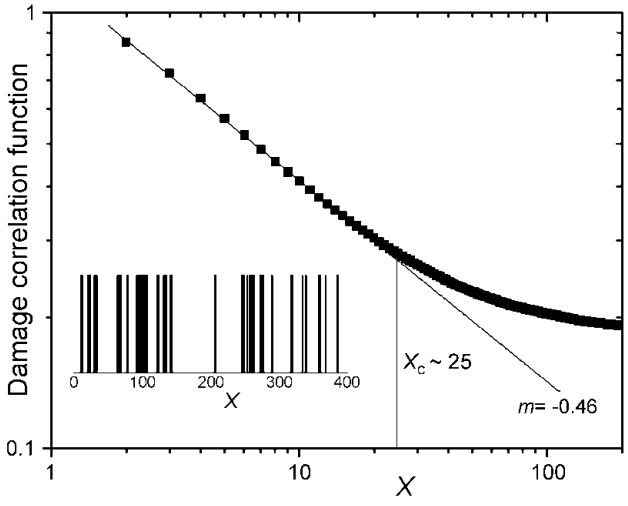

Fig. 4. Data points: two-point correlation function $C(X) = \langle D(X')D(X + X')\rangle$ of the damage pattern (average over final configurations of 1000 simulations); full line: power-law decay $C(X) \propto X^{-0.46}$. Insert: distribution of damage at failure for one system.

https://doi.org/10.3189/172756404781815040 Published online by Cambridge University Press

fractal dimension $D = (1 - m) = 0.54$. Above X_C there is a crossover to a Poissonian random pattern with fractal dimension 1. Investigation of systems of different sizes ranging between $100 \leq X_S \leq 6400$ indicates that the correlation length X_C does not depend significantly on system size.

4.4. Precursors to failure

In the presence of random strength variations, local failures may occur even before the system fails globally. In the simulations, we monitor such precursor activity by studying the displacement increments which occur after each stress increment. The insert in Figure 5 shows the increments in mean displacement which have been observed during a single simulation where the applied stress was increased in steps $\Delta T = 0.02$. One sees that the displacement increases in irregular bursts. Such bursts occur because the failure of one site may, through local stress redistribution, trigger the failure of others. (In other physical systems the term "avalanches" has become commonplace for this type of collective behavior. Here we prefer the term "bursts" for the obvious reason that we are talking about those precursor events which do *not* yet trigger an avalanche.) In real systems, such precursor events may be detectable through acoustic emission measurements and, hence, be used to gain experimental information about the internal stability of a slope.

Figure 5 shows the susceptibility $\langle \Delta U \rangle / \Delta T$ averaged over an ensemble of 10^4 systems. It is seen that the susceptibility increases as the critical stress is approached, but it does not exhibit any divergence towards failure. It is also instructive to calculate the fraction of failed sites. By analogy with equilibrium thermodynamics, this fraction may be considered an "order parameter" characterizing the failure process. This order parameter increases towards a finite value <1 as one approaches the critical stress from below, and then discontinuously jumps to unity. Hence, the behavior of the system (discontinuity of the order parameter, nonsingular behavior of the susceptibility) is reminiscent of a first-order phase transition.

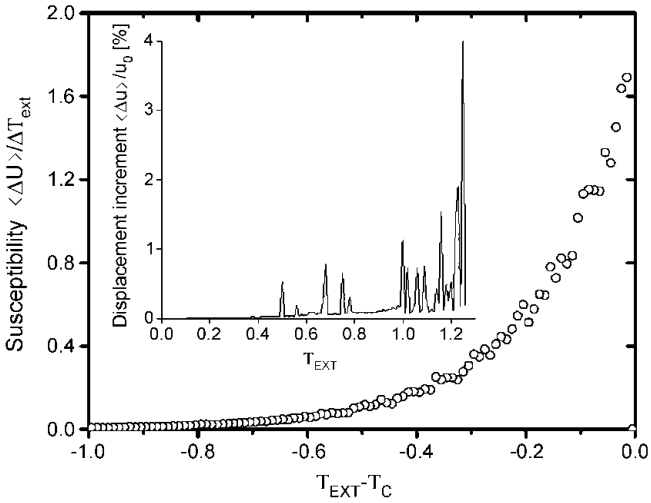

Fig. 5. Average slope susceptibility (mean displacement increment per unit stress increment, average over 10^4 simulations) as a function of distance from critical stress. Insert: displacement increments in a single simulation with step size $\Delta T = 0.02$.

5. DISCUSSION AND CONCLUSIONS

In our model of slab failure the weak layer is modelled as a softening interface. Randomness is introduced by discretizing space and assigning random peak strength values to the different "sites". Stress redistribution between strong and weak regions is expressed in terms of the (discrete) second-order gradient of the displacement, which makes the model very similar to fibre bundle models with local load sharing (Harlow and Phoenix, 1991). As in such models, we observe a first-order-like transition at failure.

From our model, the following main conclusions are drawn:

Fluctuations in the peak strength of the weak layer have a strong knock-down effect on slope stability, as stability is governed by the probability of occurrence of localized weak configurations.

The critical flaw which leads to slope failure is neither a linearly extended shear band nor a point-like deficit. Rather it falls "in between" these two extremes: prior to slope failure, the distribution of failed "sites" can, up to a characteristic correlation length, be envisaged as a fractal set of dimension $D \sim 0.5$.

As the load increases, failure is preceded by small precursor events, which may be detectable by acoustic emission as proposed, for example, by Sommerfeld and Gubler (1983). The precursor activity increases towards failure, but this increase is unspecific: since the susceptibility of the system does not diverge at the critical stress, it is difficult to pinpoint the failure stress from measurements of the precursor activity. (The situation may be compared with an attempt to determine the boiling point of a liquid from measurements of the density decrease prior to boiling.)

The present model relies on several strong idealizations which may affect the validity of our conclusions. (i) We describe stress redistribution in terms of a local load-sharing approximation. This is feasible as long as the correlation length ξ of strength variations is larger than the slab thickness. If $(d - d') > \xi$, the stress redistribution effectively leads to an averaging of the fluctuations over a region of the order of $(d - d')$. Hence, for thick slabs our model tends to overestimate the impact of fluctuations. (ii) Snow is a rate-dependent material, and the assumption of rate-independent behavior should be relaxed in future investigations. (iii) In its present form the model is quasi-one-dimensional. The assumption of homogeneity in one spatial direction is not very realistic, and, unfortunately, in statistical mechanics dimensionality matters. In the regime of large fluctuations, the behavior of the present one-dimensional model is governed by single very strong sites which may act as anchoring points for the whole slope. In two dimensions this is different since failure may bypass these sites, and ultimately the slope may avalanche, leaving the odd "super-strong" zone standing. A more detailed study of this issue is postponed to future investigations.

ACKNOWLEDGEMENTS

The author is grateful to M. Alava, J. Blackford, S. Zapperi and E. C. Aifantis for valuable discussions.

https://doi.org/10.3189/172756404781815040 Published online by Cambridge University Press

REFERENCES

Arndt, P. F. and T. Nattermann. 2001. Criterion for crack formation in disordered materials. *Phys. Rev. B*, **63**(13), 134204.

Bader, H. P. and B. Salm. 1990. On the mechanics of snow slab release. *Cold Reg. Sci. Technol.*, **17**(3), 287–300.

Conway, H. and J. Abrahamson. 1988. Snow-slope stability — a probabilistic approach. *J. Glaciol.*, **34**(117), 170–177.

Harlow, D. C. and S. L. Phoenix. 1991. Approximations for the strength distribution and size effect in an idealized lattice model of material breakdown. *J. Mech. Phys. Solids*, **39**(2), 173–200.

McClung, D. M. 1979. Shear fracture precipitated by strain softening as a mechanism of dry slab avalanche release. *J. Geophys. Res.*, **84**(B7), 3519–3526.

Palmer, A. C. and J. R. Rice. 1973. The growth of slip surfaces in the progressive failure of over-consolidated clay. *Proc. R. Soc. London, Ser. A*, **332**(1591), 527–548.

Schweizer, J. 1999. Review of dry snow slab avalanche release. *Cold Reg. Sci. Technol.*, **30**(1–3), 43–57.

Sommerfeld, R. A. and H. Gubler. 1983. Snow avalanches and acoustic emissions. *Ann. Glaciol.*, **4**, 271–276.

Wang, S. 1999. Screw dislocations in a two-phase plate and a sandwich specimen. *Physica Status Solidi, Ser. B*, **215**(2), 933–948.

Weertman, J. 1996. *Dislocation based fracture mechanics*. Singapore, World Scientific.

Zbib, H.M. and E.C. Aifantis. 1988. On the structure and width of shear bands. *Scripta Metall.*, **22**(5), 703–708.

https://doi.org/10.3189/172756404781815040 Published online by Cambridge University Press